Journal of Stress Analysis
Vol. 6, No. 1, Spring − Summer 2021, 47-60

Bu-Ali Sina University

ORIGINAL RESEARCH PAPER

Effect of Thermophoresis and Brownian Motion on Natural Convection of Yield Stress Nanofluids

M.S. Aghighi[a,*], A. Ammar[b], A. Nourbakhsh[a], H. Masoumi[a], A. Salari[a]

[a]Mechanical Engineering Department, Bu-Ali Sina University, Hamedan, Iran.

[b]Arts et Métiers ParisTech, 2 Boulevard du Ronceray, BP 93525, F-49035 Angers cedex 01, France.

Article info

Article history:
Received 02 May 2021
Received in revised form
06 August 2021
Accepted 15 August 2021

Keywords:
Viscoplastic materials
Casson model
Nanoparticles transport
Buongiorno model
Finite element method

Abstract

This paper analyzes the effects of yield stress and nanoparticles transport on the natural convection of viscoplastic Casson nanofluids. The non-linear coupled partial differential equations are solved numerically using Buongiorno's mathematical model. The governing parameters for the problem are the Rayleigh number (Ra), yield number (Y), and thermophoresis and Brownian motion parameters ($Nt\&Nb$). The effects of these parameters on the fluid flow, heat and mass transfer, and the shape of yielded and unyielded regions are examined and discussed in detail. The results demonstrate that the heat and mass transfer rates increase as the Rayleigh number increases, while the opposite behaviors are observed with increasing the yield number. The fluid is difficultly yielded at low Rayleigh number. The heat and mass transfer are primarily due to conduction at the high values of the yield number. The main effect of thermophoresis and Brownian motion parameters is on temperature and concentration distribution in the cavity. These parameters also show significant impacts on critical heat and mass transfer.

Nomenclature

B_n	Bingham number, Eq. (12)	C	Concentration, dimensionless
C_p	Specific heat capacity, kJ kg^{-1}K^{-1}	D_B	Brownian motion coefficient, m^{2}s^{-1}
D_T	Thermophoresis parameter, m^{2}s^{-1}	g	Acceleration due to gravity, ms^{-2}
H	Reference value of length, m	L	Length of the cavity, m
Le	Lewis number, Eq. (15)	m	Papanastasiou regularization parameter
Nb	Brownian motion parameter, Eq. (16)	Nr	Buoyancy ratio number, Eq. (14)
Nt	Thermophoresis parameter, Eq. (17)	Nu	Local Nusselt number, Eq. (8)
$\bar{N}u$	Average Nusselt number, Eq. (9)	p	Pressure,dimensionless
p_0	Reference value of pressure, Pa	Pr	Prandtl number, Eq. (10)
Ra	Rayleigh number, Eq. (11)	Sh	Local Sherwood number, Eq. (8)
$\bar{S}h$	Average Sherwood number, Eq. (9)	T	Temperature of fluid, K
u	Velocity component in x direction, dimensionless	v	Velocity component in y direction, dimensionless
u_0	Reference velocity, ms^{-1}	x, y	Cartesian coordinates, dimensionless
Y	Yield number, Eq. (13)		

*Corresponding author: M.S. Aghighi (Assistant Professor)
E-mail address: ms.aghighi@gmail.com
http://dx.doi.org/10.22084/jrstan.2021.24604.1182
ISSN: 2588-2597

Greek symbols			
α	Thermal diffusivity of fluid, $\mathrm{m^2s^{-1}}$	β	Coefficient of thermal expansion, $\mathrm{K^{-1}}$
$\dot{\gamma}$	Rate of strain tensor, dimensionless	θ	Temperature, dimensionless
ν	Kinematic viscosity, $\mathrm{m^2s^{-1}}$	λ	Penalty parameter, dimensionless
μ	Palstic viscosity, Pa s	ρ	Density of fluid, $\mathrm{kgm^{-3}}$
τ	Stress tensor, dimensionless	τ_y	Yield stress of fluid, dimensionless
Subscripts			
C	Cold	f	Fluid
H	Hot	r	Reference value
s	Solid particles		

1. Introduction

Natural convection heat transfer and fluid flow in a cavity have been intensively investigated by many researchers during the past decades because of its frequent presence in nature and its importance in many industrial applications such as heat exchangers, heat transfer in buildings, cooling of electronic equipment, etc. As a result, many experimental and numerical studies can be found in the literature dealing with such problems. During this period, numerous studies have been done on Newtonian fluids. An extensive review has been done by Ostrach [1]. In recent years, the analysis of this problem for nanofluids has also attracted considerable attention of many researchers due to its importance. Nanofluids are two-phase mixtures composed of nanoscale particles suspended in the base fluid with low thermal conductivity. The main feature of nanofluids is the enhancement of heat transfer derived from the high thermal conductivity of nanoparticles. However, some disadvantages, such as an increase of viscous dissipation can be mentioned in the application of nanofluids. These adverse effects are more pronounced for natural convection heat transfer [2, 3]. The study of this problem for Newtonian fluids, non-Newtonian power-law fluids, and porous media has been done by many researchers, and a good amount of work can be found in the literature, e.g. [4-10] .

Casson model was proposed by Casson [11] to describe the flow of mixtures of pigments and oil. This model is a type of viscoplastic material. It is used to describe the behavior of many materials such as blood, yogurt, tomato puree, molten chocolate, etc. [12]. Viscoplastic materials express a complex transition between solid and liquid phases. The material behaves as a solid for the stress levels below the yield stress, and above the yield stress it behaves as a viscous fluid. Many authors have extensively studied analysis of natural convection heat transfer of pure viscoplastic materials (see, for instance, Turan et al. [13], [14], Aghighi and Ammar [15], Sairamu et al. [16], Masoumi et al. [17], Rafiei et al. [18] and Aghighi et al. [19]). However, most of these works werwere based on the Bingham model, which is the simplest and most commonly used viscoplastic model. In recent years, because of the important heat transfer application of the Casson model, special attention has been devoted to deriving numerical results for this problem, among them those of Nadeem et al. [20], Hayat et al. [21, 22] and Ibrahim and Makinde [23] who considered the solution of pure and Nano Casson fluid near the stagnation point. Mehmood et al. [24] investigated the microrotation effects on mixed convection of Casson fluid induced by a stretching sheet. The effects of radiation on MHD free convection from a cylinder with partial slip in a Casson fluid in the non-Darcy porous medium was considered by Makanda et al. [25] and Raju et al. [26] analyzed MHD heat and mass transfer of Casson fluid past a stretching surface. An analysis of a Casson fluid over the oscillating plate was recently done by Mahanthesh et al. [27]. However, the bulk of the studies in this area are related to the flow over a plate or stagnation point. While, to our knowledge, there is no research dealing with the natural convection of viscoplastic Casson nanofluid in an enclosure, analysis of this problem for pure Casson fluid has been done by some authors [28-30].

The current work aims to provide a comprehensive solution of the natural convection of Casson nanofluid in a cavity with emphasis on the role of thermophoresis and Brownian motion parameters. For this purpose, a numerical model based on the finite element method was developed using the Buongiorno [31] mathematical nanofluid model. To the best of our knowledge, this problem has not been studied before and the results reported here are new and original.

2. Mathematical Formulation

Fig. 1 shows the schematic diagram and coordinate system of a two-dimensional square cavity filled with viscoplastic Casson nanofluids. The left wall is hot with a high concentration and has a constant temperature and concentration of T_H and C_H, the right wall is cold with a low concentration and has a constant temperature and concentration of T_C and C_H. The horizontal boundaries are considered to be adiabatic and impermeable. The velocity components (i.e., u for the horizontal component and v for the vertical one) are zero on the rigid walls of the cavity because of no-slip conditions. The effects of particle transport in suspensions are considered. The density variation is approximated by the Boussinesq model for both temperature and concentration. By adopting the assumptions mentioned above and introducing the characteristic scales H for length, $p_0 = (\rho_f u_0^2)$ for the pressure, and $u_0 = (g\beta H(1 - C'_r)\Delta T)^{1/2}$ for the velocity, the non-dimensional governing equations for mass, momentum, energy, and also conservation of nanoparticles based on Buongiorno's model [31] can be presented as:

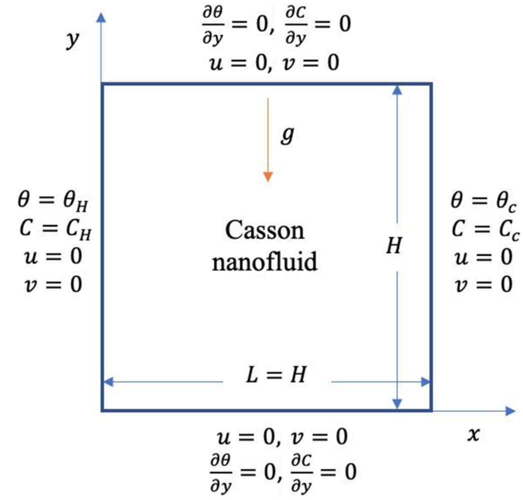

Fig. 1. Schematic diagram of the physical model and coordinate system.

$$\frac{\partial u}{\partial x} + \frac{\partial v}{\partial y} = 0$$

$$u\frac{\partial u}{\partial x} + v\frac{\partial p}{\partial y} = -\frac{\partial p}{\partial x} + Pr^{\frac{1}{2}} Ra^{\frac{-1}{2}} \left(\frac{\partial \tau_{xx}}{\partial x} + \frac{\partial \tau_{yx}}{\partial y}\right)$$

$$u\frac{\partial v}{\partial x} + v\frac{\partial v}{\partial y} = -\frac{\partial p}{\partial y} + Pr^{\frac{1}{2}} Ra^{\frac{-1}{2}} \left(\frac{\partial \tau_{yy}}{\partial y} + \frac{\partial \tau_{xy}}{\partial x}\right) + (\theta - Nr \cdot C) \tag{1}$$

$$u\frac{\partial \theta}{\partial x} + v\frac{\partial \theta}{\partial y} = (Ra \cdot Pr)^{\frac{-1}{2}} \left[\left(\frac{\partial^2 \theta}{\partial x^2} + \frac{\partial^2 \theta}{\partial y^2}\right) + N_b\left(\frac{\partial \theta}{\partial x}\frac{\partial C}{\partial x} + \frac{\partial \theta}{\partial y}\frac{\partial C}{\partial y}\right) + N_t\left(\left(\frac{\partial \theta}{\partial x}\right)^2 + \left(\frac{\partial \theta}{\partial y}\right)^2\right)\right]$$

$$u\frac{\partial C}{\partial x} + v\frac{\partial C}{\partial y} = \frac{1}{Le}(Ra \cdot Pr)^{-\frac{1}{2}} \left[\left(\frac{\partial^2 C}{\partial x^2} + \frac{\partial^2 C}{\partial y^2}\right) + \frac{N_t}{N_b}\left(\frac{\partial^2 \theta}{\partial x^2} + \frac{\partial^2 \theta}{\partial y^2}\right)\right]$$

where u, v, θ, C, and p are non-dimensional horizontal velocity, vertical velocity, temperature, concentration, and pressure, respectively.

The boundary conditions of velocity in solid walls can be written as:

$$u = 0,\ v = 0 \ \text{ on all walls} \tag{2}$$

The non-dimensional temperature θ and concentration C are defined by:

$$\theta = \frac{T - T_r}{T_H - T_C} \qquad C = \frac{C' - C'_r}{C'_H - C'_c} \tag{3}$$

Here T_r and C'_r are reference temperature and concentration: $T_r = (T_H + T_C)/2$ and $C'_r = (C'_H + C'_c)/2$.

Based on the above reference values, the relevant boundary conditions of temperature and concentration are given as follows:

$$\frac{\partial \theta}{\partial y} = 0, \quad \frac{\partial C}{\partial y} = 0 \ \text{ at } \ y = 0 \text{ and } y = 1 \tag{4}$$
$$\theta = 0.5,\ C = 0.5 \ \text{ at } \ x = 0$$
$$\theta = -0.5,\ C = -0.5 \ \text{ at } \ x = 1$$

The stress-deformation behavior of yield stress Casson fluid can be written as:

$$\tau_{ij} = \left(1 + \left(\frac{Bn}{|\dot\gamma|}\right)^{\frac{1}{2}}\right)^2 \dot\gamma_{ij} \quad \text{if} \quad |\tau| > \tau_y \quad \text{and} \qquad \dot\gamma = 0 \quad \text{for} \quad |\tau| < \tau_y \tag{5}$$

here, $|\tau|$ and $|\dot\gamma|$ are the second invariant of the shear stress and the rate of strain tensors, respectively. The component $\dot\gamma_{ij}$ of the rate-of-strain tensor is defined by:

$$\dot\gamma_{ij} = \frac{\partial u_i}{\partial x_j} + \frac{\partial u_j}{\partial x_i} \tag{6}$$

and, the rate of strain and stress tensors are given by: $|\dot\gamma| = \sqrt{\frac{1}{2}\dot\gamma_{ij}\dot\gamma_{ij}}$ and $|\tau| = \sqrt{\frac{1}{2}\tau_{ij}\tau_{ij}}$.

The Papanastasiou [32] regularization of the constitutive equation circumvents the discontinuity between yielded and unyielded regions. Hence, Eq. (5) can be rewritten as follows:

$$\tau_{ij} = \left(1 + \left(\frac{Bn}{|\dot\gamma|}\right)^{\frac{1}{2}}(1 - \exp(-\sqrt{m|\dot\gamma|})\right)^2 \dot\gamma_{ij} \tag{7}$$

In this equation, m is a regularization parameter, which allows converging to a finite value of the viscosity when $\dot\gamma \to 0$ and it provides a continuous law for the stress tensor whatever the values of $\dot\gamma$ and τ. Because the Casson model without any regularization leads to infinite viscosity when $\dot\gamma \to 0$, the value of m is usually chosen to be large; in this study, it is set to

$m = 10^4$. For this value of m, the regularized Casson model presents viscosity values close to that of the non-regularized model.

The local Nusselt and Sherwood numbers are given as follows:

$$Nu = -\left[\frac{\partial \theta}{\partial x}\right]_{x=0}$$
$$Sh = -\left[\frac{\partial C}{\partial x}\right]_{x=0} \tag{8}$$

and the mean Nusselt $\bar{Nu}$ and Sherwood $\bar{Sh}$ numbers are defined as follows:

$$\bar{Nu} = -\int_0^1 \left[\frac{\partial \theta}{\partial x}\right]_{x=0} dx$$
$$\bar{Sh} = -\int_0^1 \left[\frac{\partial C}{\partial x}\right]_{x=0} dx \tag{9}$$

The other non-dimensional parameters are defined as: Prandtl number:

$$Pr = \frac{\mu_f C_p}{K_f} \tag{10}$$

Rayleigh number:

$$Ra = \frac{g\beta(1 - C'_r)\Delta T H^3}{\alpha_f \nu_f} \tag{11}$$

Bingham number:

$$Bn = (Pr/Ra)^{-\frac{1}{2}} \frac{\tau_y}{\rho_f \beta g \Delta T H} = (Pr/Ra)^{-\frac{1}{2}} Y \tag{12}$$

Yield number:

$$Y = \frac{\tau_y}{\rho_f \beta g \Delta T H} \tag{13}$$

Buoyancy ratio number:

$$Nr = \frac{(\rho_s - \rho_f)\Delta C}{\rho_f \beta \Delta T (1 - C'_r)} \tag{14}$$

Lewis number:

$$Le = \frac{\alpha_f}{D_B} \tag{15}$$

Brownian motion parameter:

$$Nb = \frac{\delta D_B \Delta C}{\alpha_f} \tag{16}$$

Thermophoresis parameter:

$$Nt = \frac{\delta D_T \Delta T}{\alpha_f T_r} \tag{17}$$

In these equations, C_p, k, and β are the dynamic viscosity, the specific heat capacity, the thermal conductivity, and the coefficient of thermal expansion, respectively. g is the acceleration due to gravity, α is the thermal diffusivity, ΔT is the temperature difference between hot and cold walls and is the kinematic viscosity, $\Delta C'$ is the concentration difference between hot and cold walls, D_B is the Brownian motion coefficient, D_T is the thermophoresis coefficient and $\delta \frac{(\rho C_p)_s}{(\rho C_P)_f}$. Here the subscript f stands for fluid and subscript s refers to solid particles.

3. Numerical Methodology

3.1. Method of Solution

The coupled partial differential equations (Eq. 1) related to the two-dimensional laminar natural convection of viscoplastic Casson nanofluids in a cavity with differentially heated horizontal walls are discretized by developing a numerical code based on the weighted residuals finite element method. The uniform structured grid is constructed by means of nine node biquadratic elements [33].

The solution is obtained using the numerical method described in [29]. Here, this method is developed for heat and mass transfer cases by adding a concentration equation and considering its effects on momentum and energy equations. So, because of new non-linear terms, the initial (previous) values of velocity, temperature, and concentration were imposed to momentum, energy, and concentration equations to avoid nonlinearities. The solution was considered convergent when the relative error between the new and old values of velocity components and temperature and concentration fields become less than 10^{-4}.

3.2. Numerical Method Validation

A mesh analysis procedure was examined to guarantee a grid-independent solution of the present study. The grid independence of the solutions is done for $Ra = 10^6$ and $Y = 0$ (which is the most sensitive case). The results of velocity and heat and mass transfer for different meshes were obtained and compared. Based on the results, it was found that the mesh consisting of 6561 nodes guarantees a grid-independent solution within the relative tolerance level of 10^{-3}. Extensive comparisons between the present numerical method and the prior studies for pure Casson fluid are reported in the recent studies [29-30]. Additionally, the results obtained for natural convection of nanofluids in a cavity were compared qualitatively with the numerical results obtained by Sheremet et al. [34] (Fig. 2). Excellent agreement has been observed for all the results.

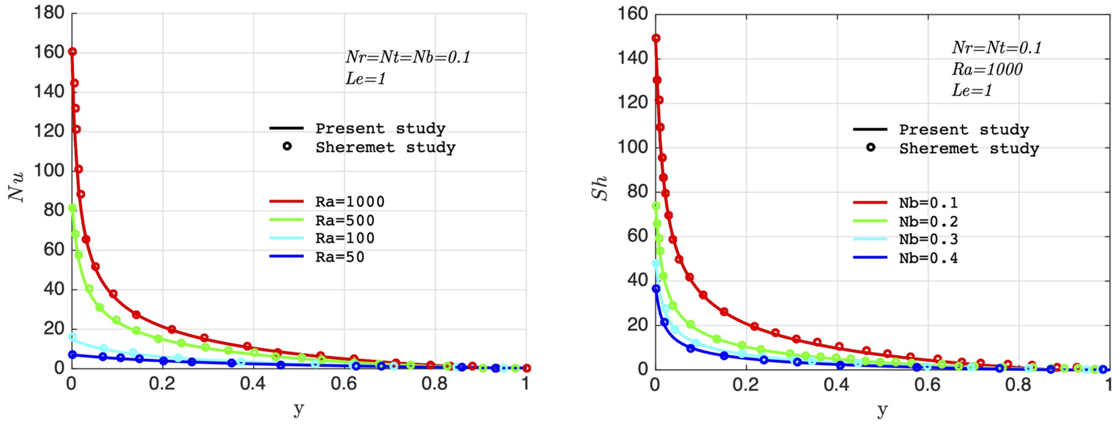

Fig. 2. Validation of the present code results for local Nusselt number Nu and local Sherwood number Sh in an enclosure with differentially heated side walls (present study and Sheremet study [32]).

4. Results and Discussion

The new extensive results on the natural convection of Casson nanofluids are presented for several values of Rayleigh number ($10^3 \leq Ra \leq 10^6$), yield number ($0 \leq Y \leq Y_{\max}$), and thermophoresis and Brownian motion parameters ($0.1 \leq N_b = N_t \leq 0.7$) at constant values of the Buoyancy ratio number ($Nr = 0.1$), Lewis number ($Le = 5$), and Prandtl number ($Pr = 10$). Efforts have been made to analyze the effects of these parameters on the fluid flow and heat and mass transfer characteristics.

4.1. Effects of Rayleigh Number

The variations of the horizontal component of velocity, u with Y along the vertical mid-plane ($x = 0.5$) and the variations of the vertical component of velocity, v, temperature, θ, and concentration, C, with Y along the horizontal mid-plane ($y = 0.5$) of the cavity are depicted in Fig. 3 for $Ra = 10^4$,10^5, 10^6. The results show that the velocity magnitude increases with increasing Ra due to stronger convection currents in the cavity. For the same reason, temperature and concentration distributions become more non-linear. Results show that at high Ra and low yield numbers, there is a strong concentration gradient close to the left and right walls, while the concentration remains uniform in a large area around the center of the cell. On the other hand, the results for increasing values of the yield number show reverse behavior due to stronger viscous resistance, which overcomes the effects of convection. Besides, the linear distributions of temperature and concentration can be seen at a high enough yield number, $Y_{\max}$, which indicates conduction-driven transport. As Ra increases, the stronger convection force can overcome the flow resistance up to greater values of the yield number. Hence, one can see that the value of $Y_{\max}$ increases with increasing Ra.

The local Nusselt and Sherwood numbers of the hot left wall have been presented in Fig. 4 for $Ra = 10^4$, 10^6. It is observed that the local Nusselt and Sherwood numbers increase with increasing Ra. As stated earlier, it is due to the stronger convective thermal transport in the cavity. In all cases, the minimum heat and mass transfer occur at the top corner, where the hot flow moves away from the hot wall. On the other hand, the maximum heat and mass transfer can be observed near the bottom corner at the point where the cold flow is in contact with the hot wall.

Results show that the heat and mass transfer decrease with increasing the yield number, and their distributions become progressively linear due to the stronger viscous resistance. The black lines in these figures present the result of simplifying the energy and concentration equations on this particular wall when the yielding number is the maximum value.

The variation of mean Nusselt and Sherwood numbers of the hot wall is shown in Fig. 5. The results are presented for different values of yield and Rayleigh number. As expected, the heat and mass transfer increase with an increase in Rayleigh number. On the other hand, as the yield number increases, the amount of heat and mass transfer decreases uniformly from its maximum for Newtonian fluid ($Y = 0$) to the minimum values at $Y = Y_{\max}$ where the heat and mass transfer is dominant by conduction ($\bar{Nu} \approx \bar{Nu}_c$ and $\bar{Sh} \approx \bar{Sh}_c$). Here, subscript c refers to the critical values of $\bar{Nu}$ and $\bar{Sh}$ obtained for the conduction-dominated regime. Results of critical Nusselt number show the deviation of nanofluid from pure fluid ($\bar{Nu}_c = 1$). This is due to the influence of thermophoresis and Brownian motion on energy and concentration equations and corresponds to the nonlinear distribution of temperature and concentration at the maximum yield number $Y = Y_{\max}$ (see Figs. 3 and 8). It is observed that at small yield numbers, $\bar{Nu}$ and $\bar{Sh}$ decrease sharply since the viscous effect is strongly improved with increasing of yield number. The uniform distribution of $\bar{Nu}$ and $\bar{Sh}$ can be seen at large values of Y because there is still a weak convective flow in the cavity that is resistant to yield stress. In this study, a relative tolerance of 10^{-3} is used as the convergence criterion for the Nusselt number.

The stream functions and contours of temperature, θ and concentration, C are presented in Fig. 6 for four different values of yield numbers at $Ra = 10^4$. Fig. 7 depicts similar results for $Ra = 10^6$. Clockwise circulation of flow in the cavity can be seen due to the buoyancy effects. Stronger fluid flow, hence the greater magnitudes of the stream functions and more curved isotherm and isoconcentration contours can be observed for higher Rayleigh numbers. On the other hand, the magnitudes of the stream functions decrease with an increase in Y, leading to more uniform temperature and concentration distributions. In these figures, the unyielded (plug) regions are represented by shaded parts. One can see that these areas increase with increasing Y due to stronger viscous effects. At a high enough yield number ($Y \cong Y_C$) the unyielded regions forming a solid plug covers the entire cavity leading to conductive heat and mass transfer. However, as mentioned earlier, there is still a weak convective flow in the cavity. The results show a high concentration gradient of particles at the left heated surface ($\bar{Sh}_c > 1$) which is accompanied by a weaker thermal gradient ($\bar{Nu}_c < 1$). Conversely, an increase in temperature gradients can be seen at the cold wall due to the low concentration.

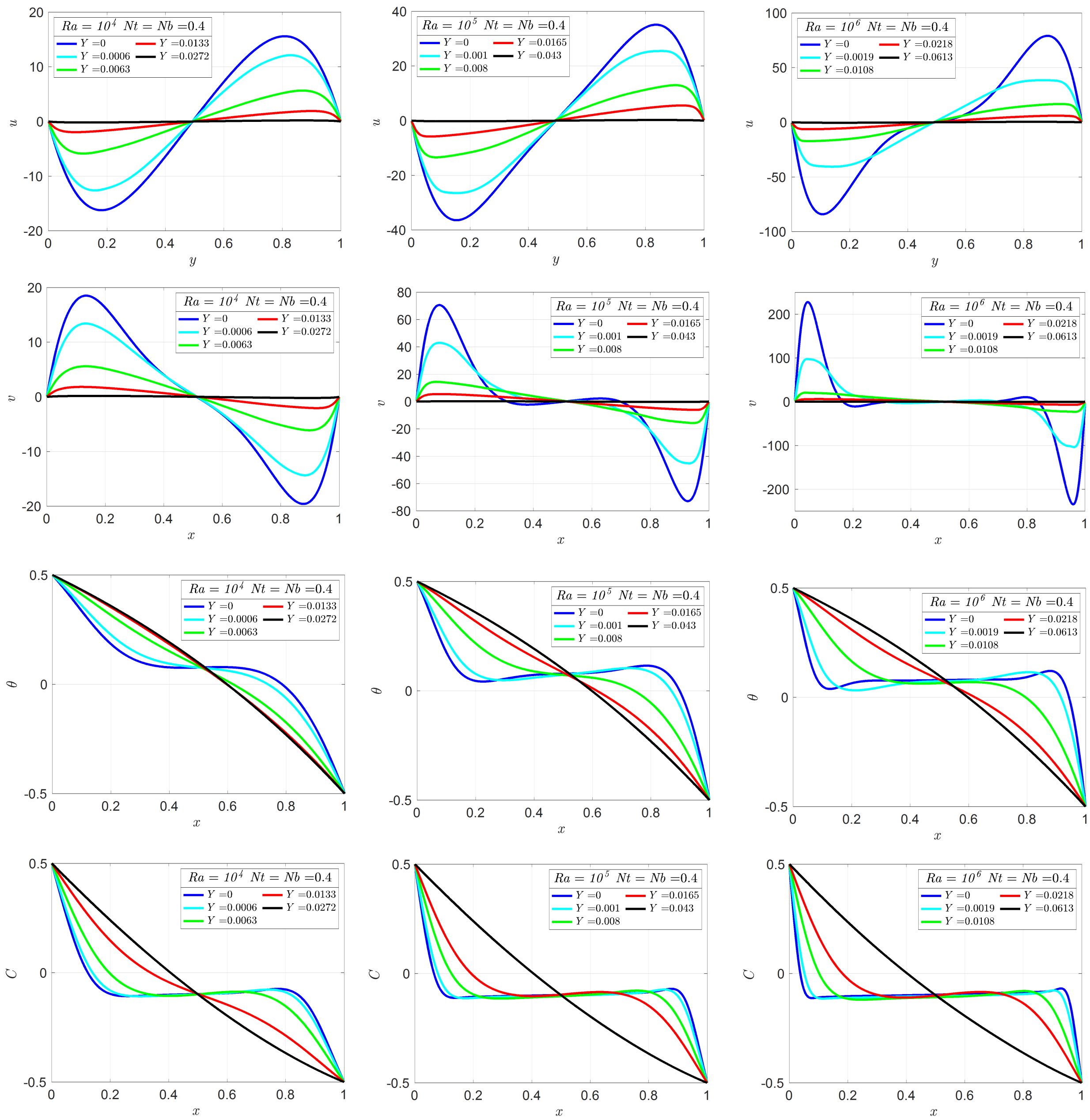

Fig. 3. Variations of non-dimensional velocity u (along the vertical mid-plane) and non-dimensional velocity v, temperature θ, and concentration C (along the horizontal mid-plane) with yield number, Y, at $Ra = 10^4$ (left), $Ra = 10^5$ (midlle) and $Ra = 10^6$ (rights) for $Nt = Nb = 0.4$, $Nr = 0.1$, $Le = 5$.

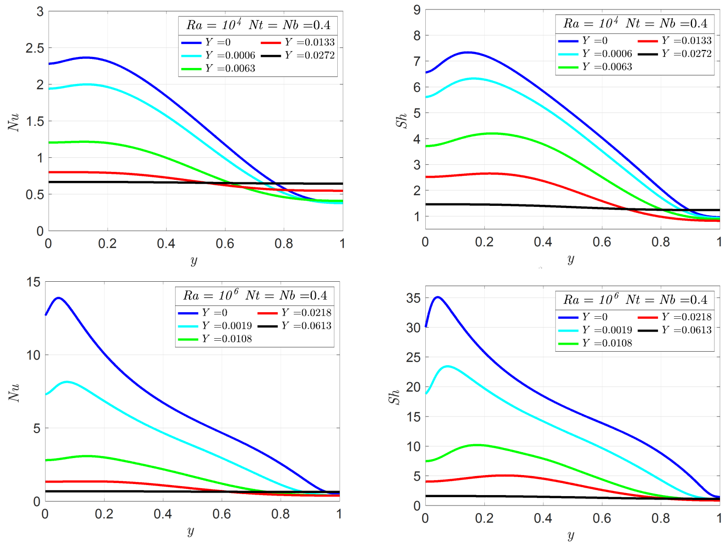

Fig. 4. Variations of local Nusselt number Nu and local Sherwood number Sh (along the hot wall) with yield number, Y, at $Ra = 10^4$ (top) and $Ra = 10^6$ (bottom) for $Nt = Nb = 0.4$, $Nr = 0.1$, $Le = 5$.

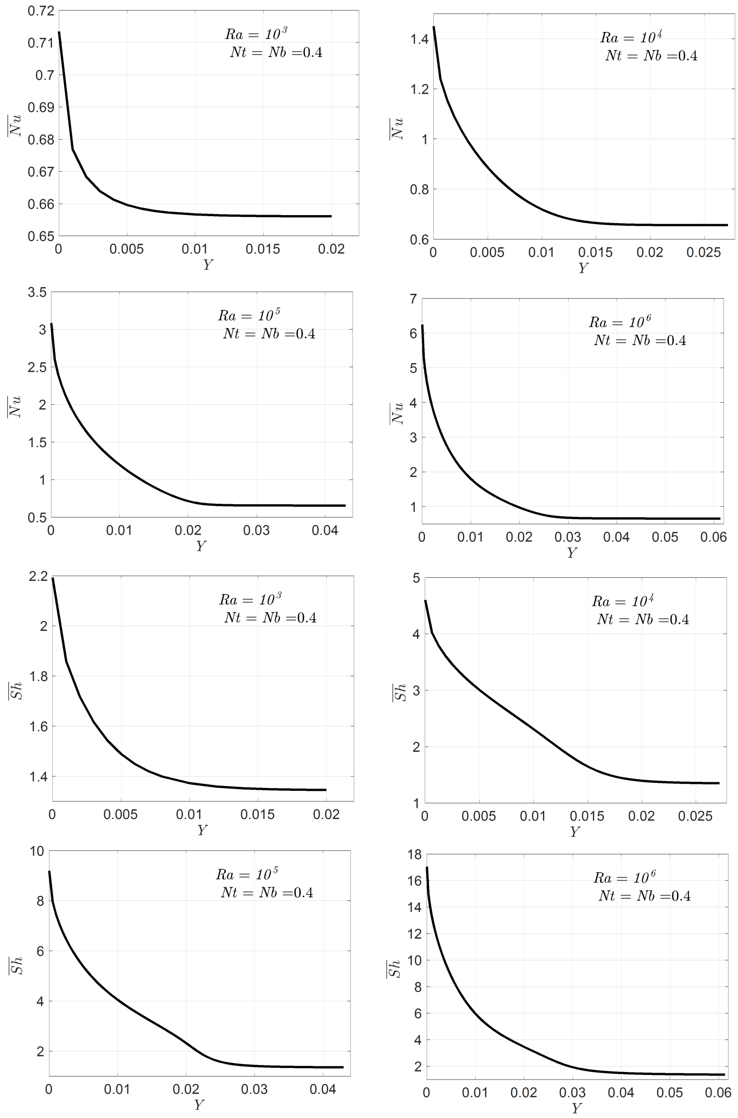

Fig. 5. Variations of mean Nusselt number $\bar{N}u$ and mean Sherwood number $\bar{S}h$ with yield number, Y, along the hot wall at $Ra = 10^3 - 10^6$ for$Nt = Nb = 0.4$, $Nr = 0.1$, $Le = 5$.

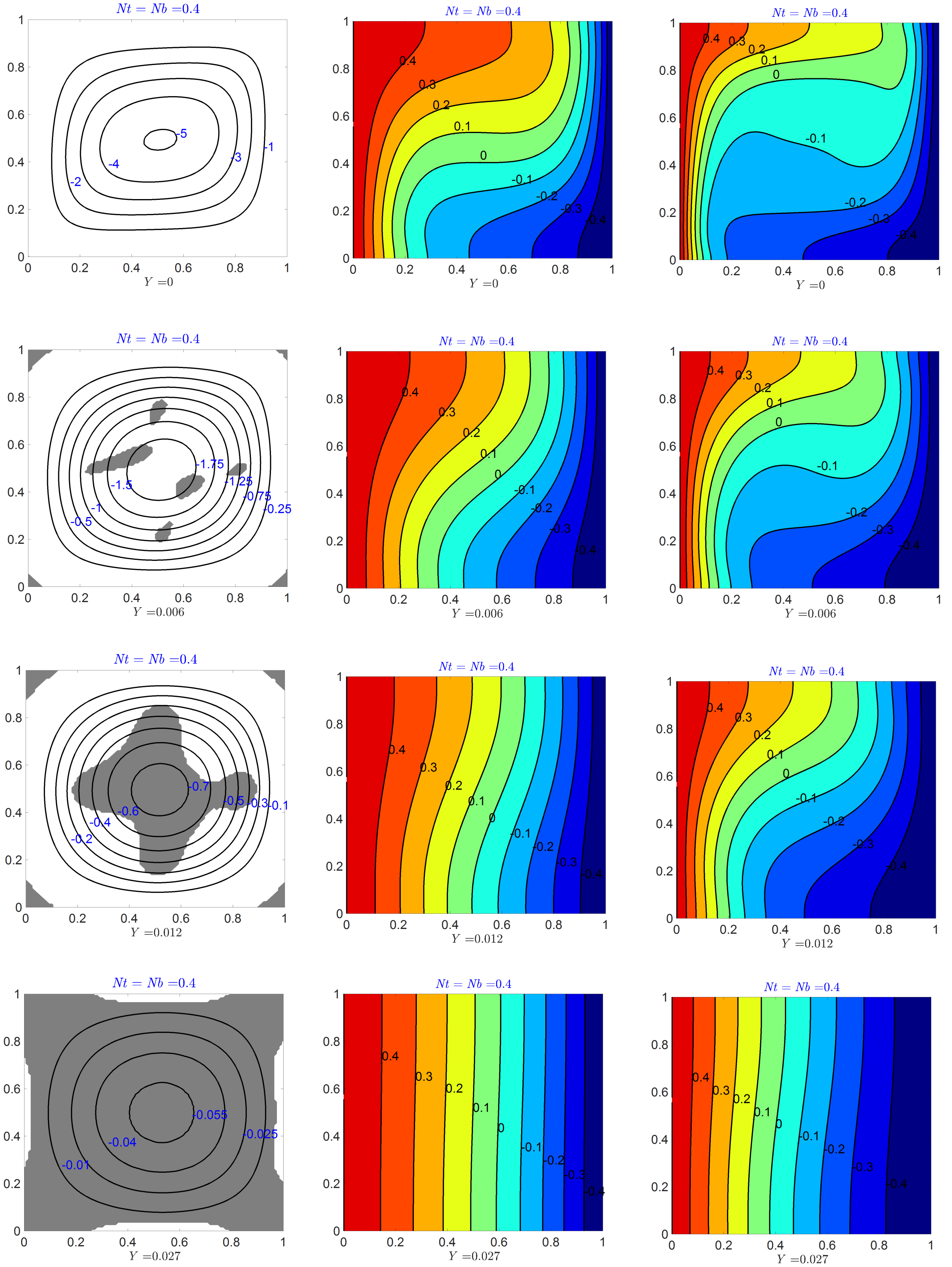

Fig. 6. Contours of non-dimensional stream functions, temperature, θ, and Concentration, C, for different values of yield number, Y, at $Ra = 10^4$ for $Nt = Nb = 0.4$, $Nr = 0.1$, $Le = 5$.

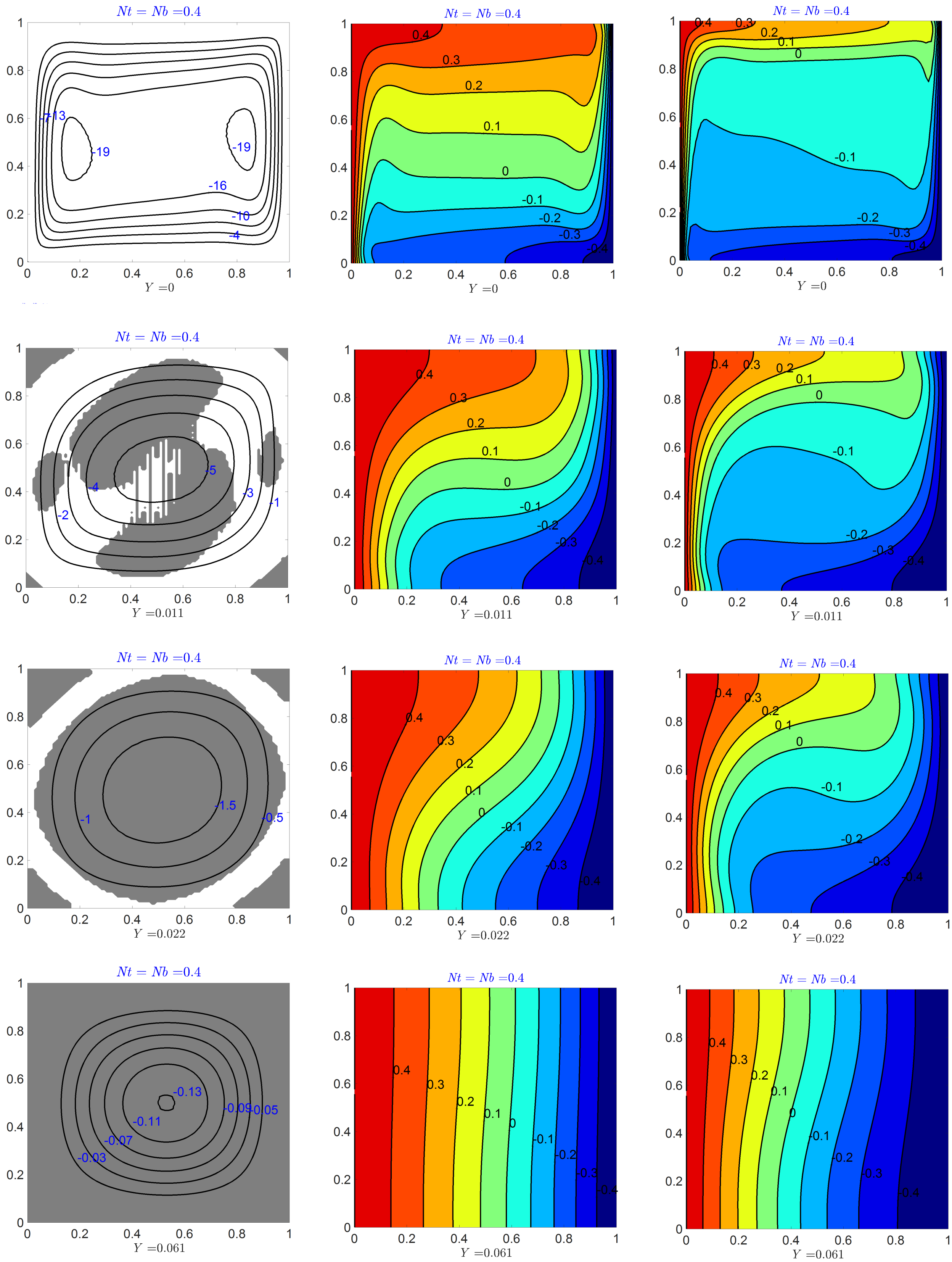

Fig. 7. Contours of non-dimensional stream functions, temperature, θ, and Concentration, C, for different values of yield number, Y, at at $Ra = 10^6$ for $Nt = Nb = 0.4$, $Nr = 0.1$, $Le = 5$.

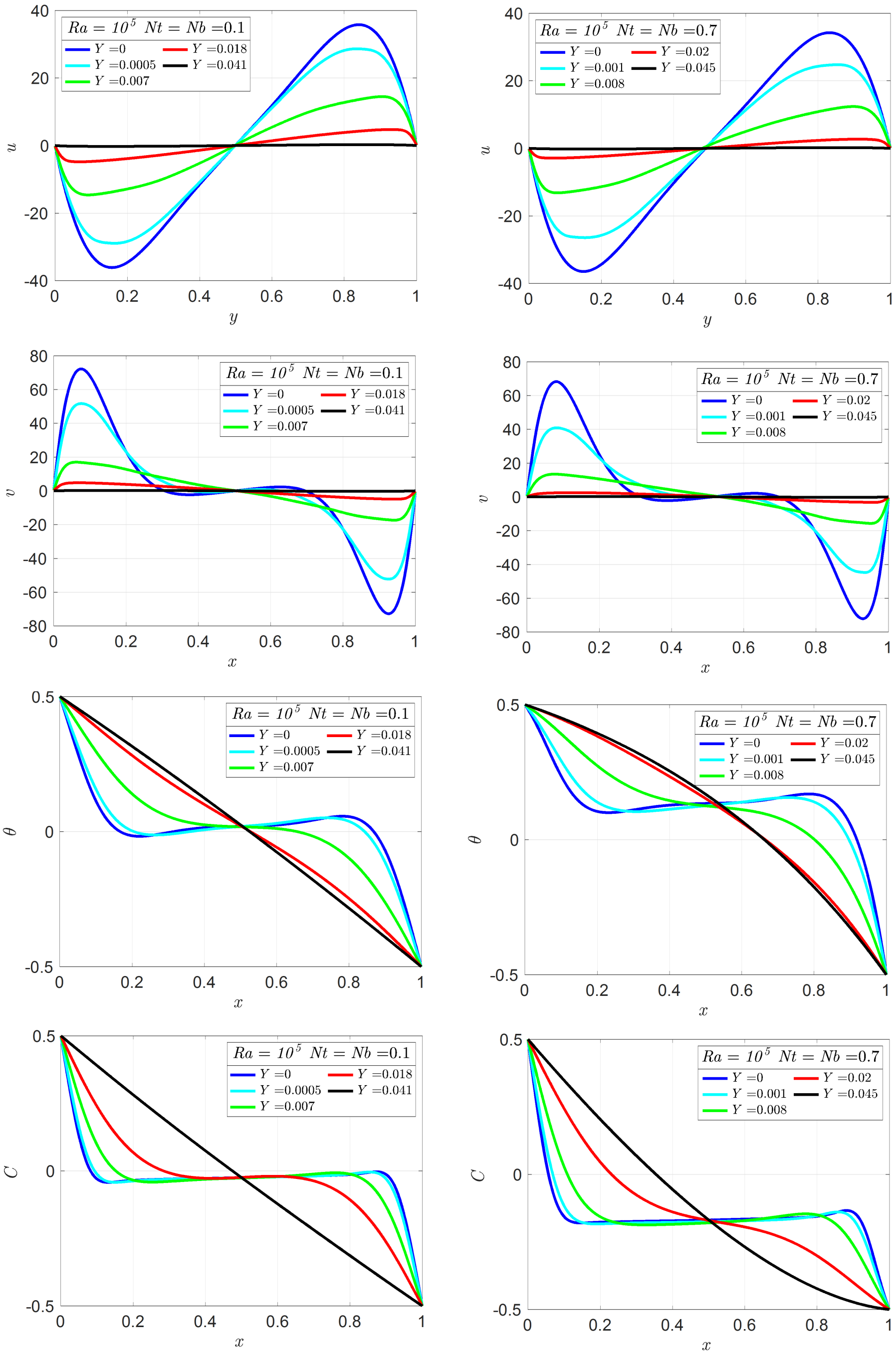

Fig. 8. Variations of non-dimensional velocity u (along the vertical mid-plane) and non-dimensional velocity v, temperature θ, and concentration C (along the horizontal mid-plane) with yield number, Y, at $Nt = Nb = 0.1$ (left), and $Nt = Nb = 0.7$ (right), for $Ra = 10^5$, $Nr = 0.1$, $Le = 5$.

4.2. Effects of Thermophoresis and Brownian Motion

The variations of velocity, temperature, and concentration with yield number for ($Nt = Nb = 0.1$), and ($Nt = Nb = 0.7$) at a representative value of nominal Rayleigh number ($Ra = 10^5$) are shown in Fig. 8. Slip velocity mechanisms of nanoparticles in nanofluids can be explained by Brownian motion and thermophoresis parameters. The nanoparticles near the hot wall carry greater kinetic energy (thermophoretic). On the other hand, the random and fluctuating motion of particles increases by increasing the Brownian motion parameter. The opposite phenomenon is observed in the vicinity of the cold wall. Hence, it can be seen from Fig. 8 that the increase in the value of these parameters leads to non-uniform distribution of temperature and concentration while no significant change is found in the flow pattern. The results show that the concentration gradient increases at the hot wall and decreases near the cold border. An opposite behavior can be observed for temperature distribution while the fluid velocity and critical yield number are not significantly affected by Nt and Nb.

Fig. 9 shows the local Nusselt and Sherwood numbers for different yield numbers at $Nt = Nb = 0.4$ (left) and $Nt = Nb = 0.7$ (right). The mean values of these quantities are shown in Fig. 10.

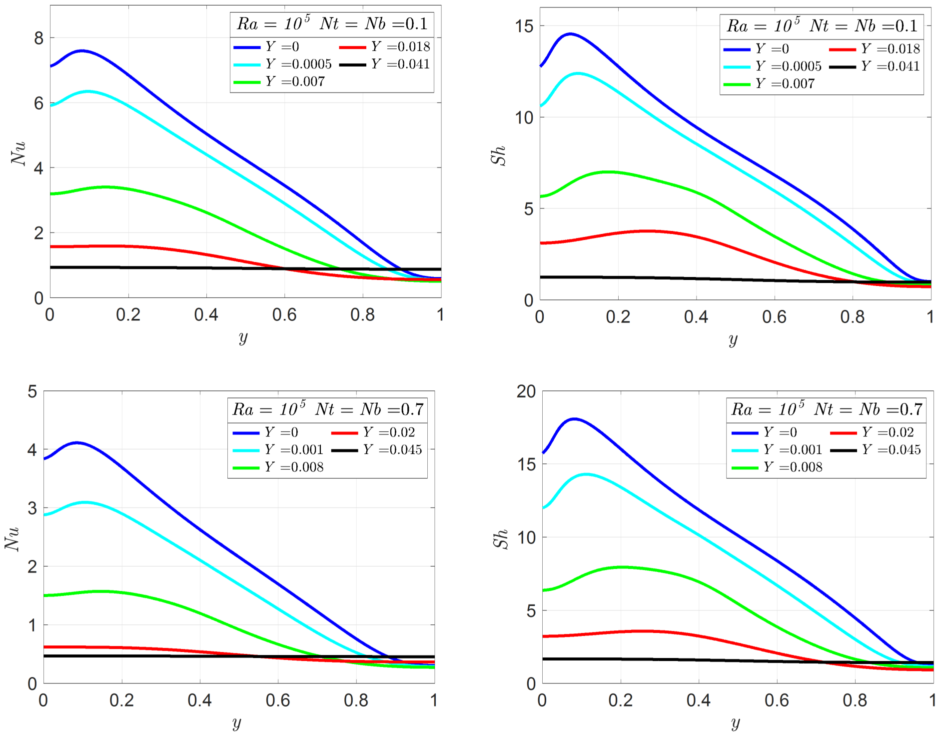

Fig. 9. Variations of local Nusselt number Nu and local Sherwood number Sh (along the hot wall) with yield number, Y, at $Nt = Nb = 0.1$ (top) and $Nt = Nb = 0.7$ (bottom), for $Ra = 10^5$, $Nr = 0.1$, $Le = 5$.

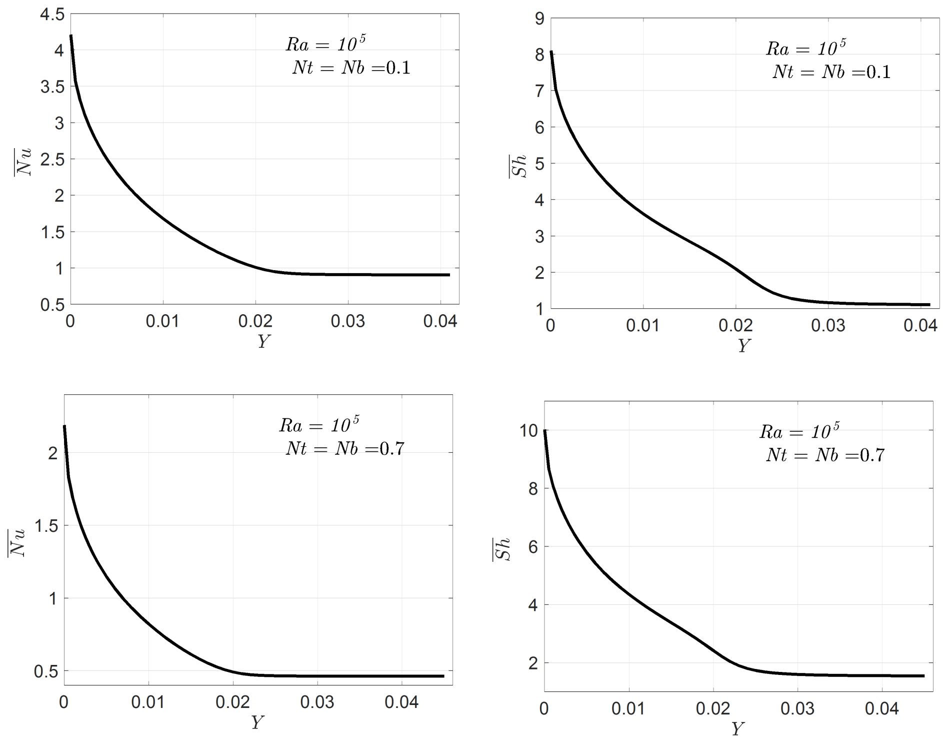

Fig. 10. Variations of mean Nusselt number $\bar{N}u$ and mean Sherwood number $\bar{S}h$ (along the hot wall) with yield number, Y, at $Nt = Nb = 0.1$ (top) and $Nt = Nb = 0.7$ (bottom), for $Ra = 10^5$, $Nr = 0.1$, $Le = 5$.

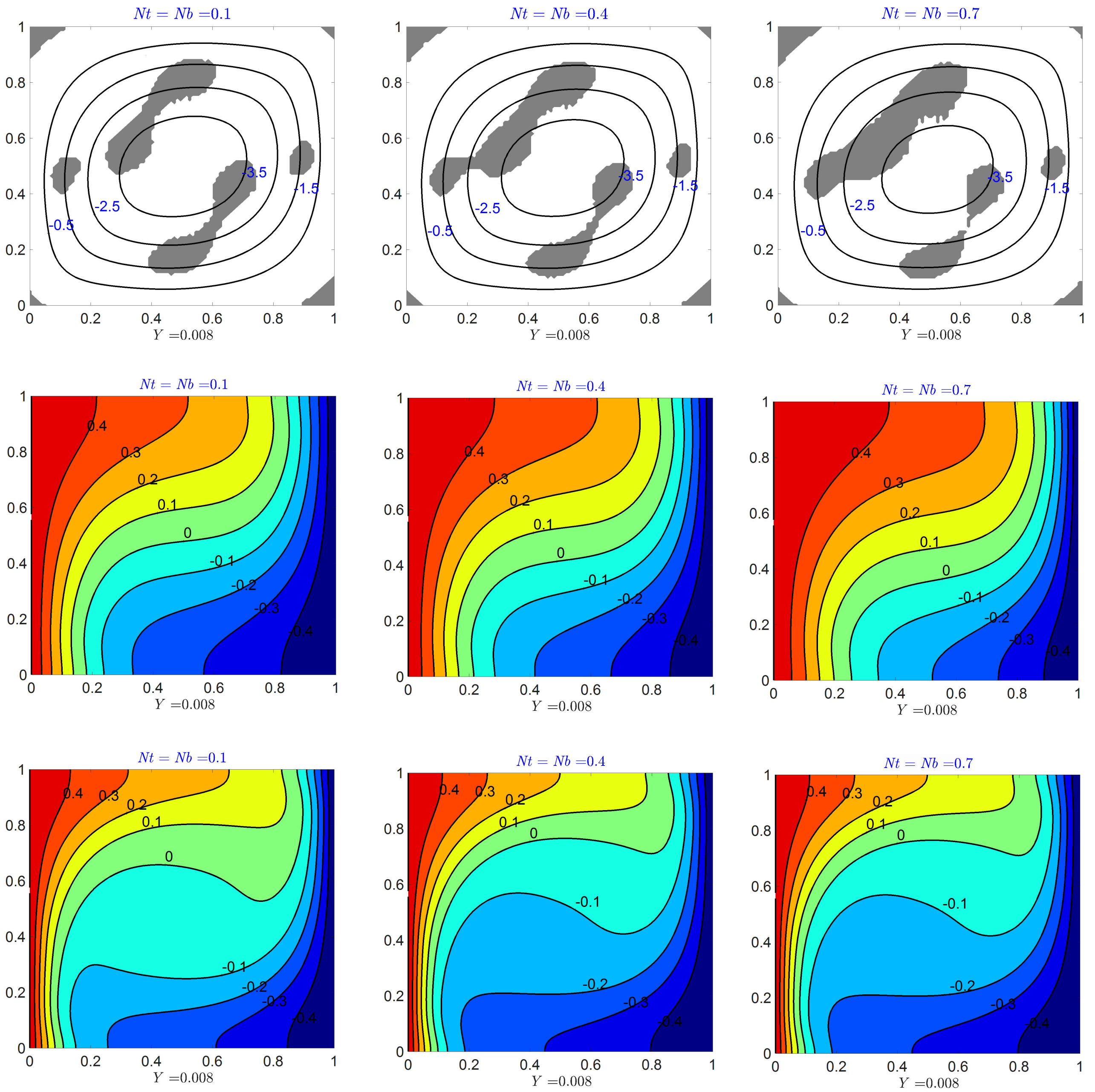

Fig. 11. Contours of non-dimensional stream functions, temperature, θ, and Concentration, C, for different values of Brownian motion and thermophoresis, Nt and Nb, at $Ra = 10^5$ and $Y = 0.008$ for $Nr = 0.1$, $Le = 5$.

As mentioned before, as the Brownian motion and thermophoresis increase, the concentration gradient on the hot wall increases while the thermal gradient decreases. Hence, in accordance with the temperature and concentration profiles enforced at the hot wall, it can be seen that the Nusselt number decreases with increasing values of Nt and Nb while the Sherwood number increases. It is worth mentioning here that thermophoresis and Brownian motion parameters also have significant impacts on $\bar{N}u_c$ and $\bar{S}h_c$. However, in all cases, heat and mass transfer decrease with increasing the yield number due to the stabilizing influence of the fluid yield stress. Increasing the values of Brownian motion and thermophoresis parameters cause nanoparticles to accumulate in the hot wall, which is accompanied by the enlarged isothermal zone (Fig. 11). However, no significant changes are seen in stream functions. Results show that the plug regions grow in the upper- left area of the cavity, where the higher gradients of nanoparticles can be seen.

5. Conclusions

In this work, the natural convection of viscoplastic Casson nanofluids has been studied numerically in a square enclosure using Buongiorno's model. The system of nonlinear differential equations has been solved numerically using Galerkin finite element method.

The Casson model, as part of viscoplastic materials, provides a link between solid and fluid behavior. In fact, they represent solids with low yield stresses which can flow like a fluid at the greater applied stress. Therefore, the most important parameter in analyzing their behavior is yield stress. Our study showed that the combined effect of yield stress and nanoparticles properties strongly affects the performance of these materials and their conversion from liquid to solid and vice versa. Actually, the increase in the yield stress leads to reduced heat and mass transfer and as a result, it causes the fluid to solidify.

The study of the effects of thermophoresis and Brownian motion parameters on yield stress nanofluid shows that these parameters have a more pronounced effect on the heat and mass transfer than it does on the fluid flow. The main impact of these parameters was observed in the non-uniform distribution of temperature and concentration. It can be seen that the concentration gradient increases at the hot wall and decreases near the cold wall. An opposite behavior can be observed for temperature distribution. These parameters also have significant impacts on $(\bar{Nu}_c)$ and $(\bar{Sh}_c)$. A detailed examination of the results reveals the effect of thermophoresis and Brownian motion parameters on the distribution of unyielded areas in such a way that unyielded regions increase with increasing Nt and Nb.

Acknowledgment

This research did not receive any specific grant from funding agencies in the public, commercial, or not-for-profit sectors.

References

[1] S. Ostrach, Natural Convection in Enclosures. ASME. J. Heat Transfer., 110(4b) (1988) 1175-1190.

[2] M. Corcione, Rayleigh-Bénard convection heat transfer in nanoparticle suspensions, Int. J. Heat Fluid Flow, 32(1) (2011) 65-77.

[3] S. Aghighi, A. Ammar, C. Metivier, F. Chinesta, Parametric solution of the Rayleigh-Benard convection model by using the PGD, Int. J. Numer. Methods Heat Fluid Flow, 25(6) (2015) 1252-1281.

[4] H.F. Oztop, E. Abu-Nada, Numerical study of natural convection in partially heated rectangular enclosures filled with nanofluids, Int. J. Heat Fluid Flow, 29(5) (2008) 1326-1336.

[5] O. Abouali, G. Ahmadi, Computer simulations of natural convection of single phase nanofluids in simple enclosures: A critical review, Appl. Therm. Eng., 36 (2012) 1-13.

[6] F. Garoosi, S. Garoosi, K. Hooman, Numerical simulation of natural convection and mixed convection of the nanofluid in a square cavity using Buongiorno model, Powder Technol., 268 (2014) 279-292.

[7] G.C. Bourantas, V.C. Loukopoulos, Modeling the natural convective flow of micropolar nanofluids, Int. J. Heat Mass Transf., 68 (2014) 35-41.

[8] G.H.R. Kefayati, Heat transfer and entropy generation of natural convection on non-Newtonian nanofluids in a porous cavity, Powder Technol., 299 (2016) 127-149.

[9] A.I. Alsabery, A.J. Chamkha, H. Saleh, I. Hashim, Transient natural convective heat transfer in a trapezoidal cavity filled with non-Newtonian nanofluid with sinusoidal boundary conditions on both sidewalls, Powder Technol., 308 (2017) 214-234.

[10] S.A.M. Mehryan, M. Ghalambaz, A.J. Chamkha, M. Izadi, Numerical study on natural convection of Ag-MgO hybrid/water nanofluid inside a porous enclosure: A local thermal non-equilibrium model, Powder Technol., 367 (2020) 443-455.

[11] N. Casson, Rheology of Disperse Systems, Pergamon Press, Oxford, (1959).

[12] R.P. Chhabra, J.F. Richardson, Non-Newtonian Flow and Applied Rheology: Engineering Applications, Butterworth-Heinemann/Elsevier, (2008).

[13] O. Turan, N. Chakraborty, R.J. Poole, Laminar natural convection of Bingham fluids in a square enclosure with differentially heated side walls, J. Nonnewton, Fluid Mech., 165(15-16) (2010) 901-913.

[14] O. Turan, N. Chakraborty, R.J. Poole, Laminar Rayleigh-Bénard convection of yield stress fluids in a square enclosure, J. Nonnewton. Fluid Mech., 171-172 (2012) 83-96.

[15] M.S. Aghighi, A. Ammar, Aspect ratio effects in Rayleigh-Bénard convection of Herschel-Bulkley fluids, Eng. Comput., 34(5) (2017) 1658-1676.

[16] M. Sairamu, N. Nirmalkar, R.P. Chhabra, Natural convection from a circular cylinder in confined Bingham plastic fluids, Int. J. Heat Mass Transf., 60 (2013) 567-581.

[17] H. Masoumi, M.S. Aghighi, A. Ammar, A. Nourbakhsh, Laminar natural convection of yield stress fluids in annular spaces between concentric cylinders, Int. J. Heat Mass Transf., 138 (2019) 1188-1198.

[18] B. Rafiei, H. Masoumi, M.S. Aghighi, A. Ammar, Effects of complex boundary conditions on natural convection of a viscoplastic fluid, Int. J. Numer. Methods Heat Fluid Flow, 29(8) (2019) 2792-2808.

[19] M.S. Aghighi, A. Ammar, H. Masoumi, A. Lanjabi, Rayleigh-Bénard convection of a viscoplastic liquid in a trapezoidal enclosure, Int. J. Mech. Sci., 180 (2020) 105630.

[20] S. Nadeem, R. Mehmood, N.S. Akbar, Optimized analytical solution for oblique flow of a Casson-nano fluid with convective boundary conditions, Int. J. Therm. Sci., 78 (2014) 90-100.

[21] T. Hayat, S.A. Shehzad, A. Alsaedi, M.S. Alhothuali, Mixed convection stagnation point flow of Casson fluid with convective boundary conditions, Chinese Phys. Lett., 29(11) (2012) 114704.

[22] T. Hayat, M. Farooq, A. Alsaedi, Thermally stratified stagnation point flow of Casson fluid with slip conditions, Int. J. Numer. Methods Heat Fluid Flow, 25(4) (2015) 724-748.

[23] W. Ibrahim, O.D. Makinde, Magnetohydrodynamic stagnation point flow and heat transfer of Casson nanofluid past a stretching sheet with slip and convective boundary condition, J. Aerosp. Eng., 29(2) (2016) 04015037.

[24] Z. Mehmood, R. Mehmood, Z. Iqbal, numerical investigation of micropolar Casson fluid over a stretching sheet with internal heating, Commun. Theor. Phys., 67(4) (2017) 443-448.

[25] G. Makanda, S. Shaw, P. Sibanda, Effects of radiation on MHD free convection of a Casson fluid from a horizontal circular cylinder with partial slip in non-Darcy porous medium with viscous dissipation, Bound. Value Probl., 2015 (2015) 75.

[26] C.S.K. Raju, N. Sandeep, V. Sugunamma, M. Jayachandra Babu, J.V. Ramana Reddy, Heat and mass transfer in magnetohydrodynamic Casson fluid over an exponentially permeable stretching surface, Eng. Sci. Technol. Int. J., 19(1) (2016) 45-52.

[27] B. Mahanthesh, T. Brizlyn, S.A. Shehzad, G. B.J., Nonlinear thermo-solutal convective flow of Casson fluid over an oscillating plate due to non-coaxial rotation with quadratic density fluctuation: Exact solutions, Multidiscip. Model. Mater. Struct., 15(4) (2019) 818-842.

[28] I. Pop, M. Sheremet, Free convection in a square cavity filled with a Casson fluid under the effects of thermal radiation and viscous dissipation, Int. J. Numer. Methods Heat Fluid Flow, 27(10) (2017) 2318-2332.

[29] M.S. Aghighi, A. Ammar, C. Metivier, M. Gharagozlu, Rayleigh-Bénard convection of Casson fluids, Int. J. Therm. Sci., 127 (2018) 79-90.

[30] M.S. Aghighi, C. Metivier, H. Masoumi, Natural convection of Casson fluid in a square enclosure, Multidiscip. Model. Mater. Struct., 16(5) (2020) 1245-1259.

[31] J. Buongiorno, Convective transport in nanofluids, J. Heat Transfer., 128(3) (2006) 240-250.

[32] T.C. Papanastasiou, Flows of materials with yield, J. Rheol., 31(5) (1987) 385-404.

[33] G. Dhatt, G. Touzot, E. Lefrançois, Finite Element Method, ISTE Ltd and John Wiley & Sons, Inc. London, (2012).

[34] M.A. Sheremet, T. Groşan, I. Pop, Steady-state free convection in right-angle porous trapezoidal cavity filled by a nanofluid: Buongiorno's mathematical model, Eur. J. Mech. B/Fluids, 53 (2015) 241-250.